Light metals on oxygen-terminated diamond (100): structure and electronic properties

Kane M. O'Donnell,*,§ Tomas L. Martin¶ and Neil L. Allan#

§Department of Imaging and Applied Physics, Curtin University, Bentley WA 6102 Australia

¶Department of Materials, University of Oxford, Parks Road, Oxford OX1 3PH United Kingdom

#Centre for Computational Chemistry, School of Chemistry, University of Bristol, Cantock's Close, Bristol BS8 1TS United Kingdom

KEYWORDS diamond, surface chemistry, negative electron affinity, adsorption, density functional theory

ABSTRACT: Recently a lithiated C(100)-(1x1):O surface has been demonstrated to possess a true negative electron affinity, i.e. the conduction band minimum at the surface is lower in energy than the local vacuum level. Here we present a density functional theory study of diamond surfaces with various alkali-metal- and alkaline-earth-oxide terminations. We find a size-dependent variation of electronic surface properties that divides the adsorbates into two groups. In both cases, ether bridges are broken. Adsorption of the smaller alkali metals/alkaline earths such as lithium and magnesium leads to a significant surface dipole resulting from transfer of charge across X-O-C complexes, whereas at the other extreme, caesium-adsorbed and potassium-adsorbed C(100)-(1x1):O surfaces exhibit conventional dipole formation between the ionic adsorbate and a negatively charged carbonyl-like surface. Sodium is intermediate. Computed surface band structures and density of states are presented illustrating the key electronic differences between these two groups.

The ability for certain diamond surfaces to exhibit a negative electron affinity (NEA) has been of great interest since its discovery by Himpsel in 1979.[1] The significantly increased electron yield of true NEA diamond is highly desirable for applications such as current amplifiers[2-4], vacuum electronics[5], thermionic converters[6] and even new forms of photochemistry[7]. Furthermore, the concomitant reduction in ionization energy with increasingly negative electron affinity is critical for surface transfer doping[8-11] used in many diamond electronic devices. For a material to have a true negative electron affinity, the conduction band minimum (CBM) at the surface must be higher in energy than the local vacuum level E_{vac}. For narrow band gap semiconductors this is difficult to achieve. Conversely, for wide band gap semiconductors such as diamond, where the conduction band minimum is naturally close to the vacuum level a suitable surface termination can alter the surface dipole sufficiently that the CBM lies above E_{vac}.[12,13] It has long been known that hydrogen-terminated diamond surfaces with {100} or {111}-orientation exhibit true negative electron affinity as demonstrated by total photoyield spectroscopy (TPYS), photoemission spectroscopy and Kelvin probe measurements.[11,12,14-16]

Until recently, only the hydrogen-terminated surface on diamond was known to exhibit a true NEA. Numerous other diamond surface modifications have been studied with the aim of finding alternative NEA diamond surfaces (for example refs [17-20]) but apart from lithium discussed below none are known to exhibit true (as opposed to effective) negative electron affinity. A surface with effective NEA has, in fact, a positive electron affinity but there is sufficient downward band-bending towards the surface within the material such that deep in the bulk the CBM is above the vacuum level. If the space charge region is narrow enough electrons are able to tunnel from the CBM through the space charge region into vacuum without encountering a barrier. The electron emission properties characteristic of a true NEA surface are also partially exhibited by effective NEA surfaces and it is easy to mistake the two.[21] Effective NEAs can be observed on a wide range of highly p-doped semiconductor materials (where the bulk Fermi level is strongly pinned near the valence band) with a surface coating such as caesium oxide that alters the Fermi level at the surface. Nevertheless, it is preferable to find methods to induce true NEA on diamond because the electron yield is significantly higher.

We have previously investigated the adsorption of lithium onto both clean and oxygenated diamond by computational methods and concluded that for the lowest-energy structures there is a large shift in ionization energy and electron affinity.[22] For lithium adsorption on the C(100)-(1x1):O surface in particular, the large adsorption energy combined with the predicted true negative electron affinity make the surface highly promising as an alternative to hydrogen-terminated diamond.

Recently such a lithiated surface was demonstrated experimentally, highlighting the need to further investigate diamond surfaces that are potential alternatives to hydrogen-terminated diamond.[13,23] Theoretical work also suggests that lithiated diamond has advantages over hydro-

gen-terminated diamond for field emission devices.[24] Lithium, carbon and oxygen are relatively small species compared to the heavier alkali metals typically used for reducing the workfunction of surfaces and it is not immediately obvious that such surfaces will have the same properties as the caesiated surface. This study explores the interaction of the series of alkali metals lithium, sodium, potassium and caesium with the C(100)-(1x1):O surface and in addition the alkaline earth metal magnesium, which often exhibits similar chemistry to lithium. A clear difference is found between lithium/magnesium and the heavier alkalis, both in terms of adsorption energy, surface dipole structure and the shift in ionization energy/electron affinity. We illustrate these differences with band structure calculations that show the interaction of the adsorbate with the electronic structure of the underlying surface.

COMPUTATIONAL METHOD

All calculations were performed using the CASTEP density functional theory code.[25] A plane wave cutoff energy of 588 eV was used throughout, with the exchange-correlation functional approximated using the revised Perdue, Burke and Emzerhof (RPBE) generalized gradient approximation.[26] The highly-cited RPBE functional is known to lead to better agreement between calculated and experimental chemisorption energies for atoms and molecules on surfaces and is an improvement upon the PW91 functional used in our previous study. The simulations used a thin slab, periodic in two dimensions and terminated on both sides by the C(100) surface. The surface unit cell in most cases was 2x1 but a 2x2 unit cell was used to allow lower coverages for the heavier alkali metals and in all cases for band structure calculations. The slab consisted of 24 carbon layers and a vacuum gap of approximately 26 Å, both converged such that the change in computed ionization energy was less than 0.1 eV. Here as elsewhere coverage is defined with respect to the number of available surface sites; hence one monolayer corresponds to one adsorbate atom per surface oxygen atom. The Brillouin zone was sampled using a Monkhorst-Pack[27] grid of 8x6x1 k-points, with symmetry leading to an explicit consideration of 24 k-points in total. Structures were optimized to minimize forces to less than 0.02 eV/Å. Density of states calculations were carried out using the OptaDOS code[28] on a k-point grid of 40x20x1 k-points and using adaptive broadening with a width of 1.0 eV.

Adsorption energies are calculated with respect to the ether bridge C(100)-(1x1):O surface [Figure 1(a)]. Although the experimental evidence is mixed (e.g. refs [29,30]), there is tentative agreement in the literature that this structure is the lowest-energy ideal C(100)-(1x1):O structure and is therefore the appropriate energetic ground state.[22,31-34] The adsorption energy per atom is then given by:

$$E_{ads} = \left(E_T - E_0 - N_{ads}E_{iso}\right)/N_{ads} \quad (1)$$

where E_T is the total energy of the supercell, E_0 is the total energy of the bare oxygen-terminated surface supercell, N_{ads} is the number of adsorbates in the supercell and E_{iso} is the energy of an isolated adsorbate atom. The computed values of E_T, E_0 and E_{ads} are negative, thus the sign convention in this work is that exothermic adsorption energies are negative.

The ionization energy for each surface was calculated using the method of Fall, et al.[35] The energy separation between the average electrostatic potential energy in the bulk and the bulk valence band maximum ($E_{VBM,bulk} - V_{av,bulk}$) is obtained from a calculation on a bulk diamond primitive unit cell. Next, a slab calculation is used to determine the energy separation between the average slab potential and the vacuum potential ($E_{VAC} - V_{av,slab}$). Combining these gives the energy from the vacuum level to the valence band maximum and thus the ionization energy, I:

$$I = (E_{VAC} - V_{av,slab}) - (E_{VBM,bulk} - V_{av,bulk}) \quad (2)$$

The sign convention here is that ionization energy is positive as for workfunction. Calculating the workfunction for semiconductors is more complex; dopants and surface states lead to the Fermi level typically being positioned away from the centre of the band gap. In contrast, the ionization energy depends only on the surface valence band maximum, provided the Fermi level lies within the band gap. From the ionization energy one can compute the electron affinity (χ) by *subtracting* the experimental bulk band gap (Eg=5.5 eV[36]). Consequently if the ionization energy is less than the band gap, the electron affinity will be negative. This can lead to ambiguity in language when comparing electron affinities both in sign and magnitude. However, in the present study *all* the surfaces apart from the clean oxygen termination have NEA. To avoid confusion, we compare the electron affinities of surfaces on the basis of the size of the NEA only, with larger meaning *more* negative.

RESULTS

1. Structures and Coverage

Figure 1 shows the lowest energy structures of highest coverage possible for Li (reference), Mg, Na, K and Cs. Further relevant structures are shown in Figure 2. Each top view (looking along [001]) shows a 2x2 unit cell. The maximum coverage changes with adsorbate size because for the larger alkalis, lattice mismatch and adsorbate interactions make it energetically unfavorable to chemically saturate the surface, i.e., coverages above a certain value are thermodynamically unstable ($E_{ads} > 0$). Hence it is necessary to consider structures in a larger supercell at lower coverages, for which there are more geometrical possibilities. At monolayer coverage there is no ambiguity about the cell periodicity but 0.5ML coverage adsorbates can form row structures leading to a 2x1 adsorbate periodicity, or off-diagonal structures leading to a √2x√2 structure. We note further that, depending on both the adsorbate and on coverage, there may or may not be a dimer reconstruction underneath the adsorbate and oxygen layers as can be seen from the side views along [110] in Figures 1 and 2. Thus, the exact classification of the surface symmetry is somewhat more involved than simply specifying the symmetry of the adsorbates.

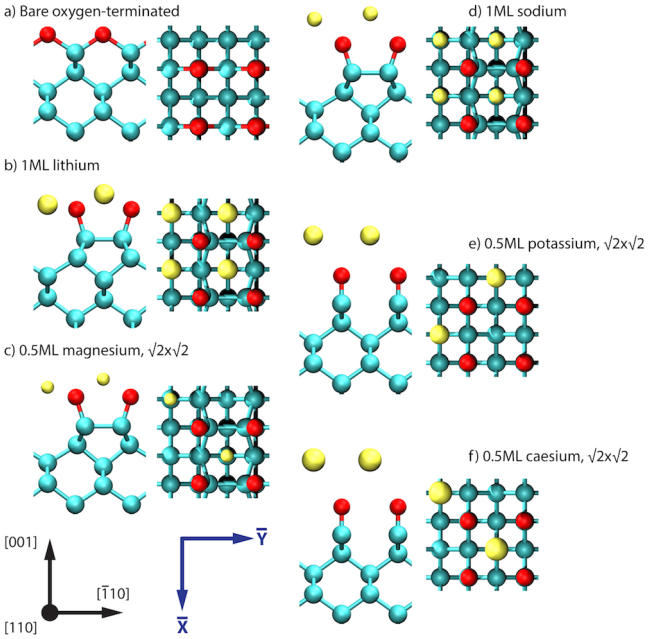

Figure 1. Stable high coverage structures considered in this work. (a) Reference oxygen termination of ether-bridge structure, (b) 1ML Li as previously reported,[22] (c) 0.5ML Mg-adsorbed surface in the √2x√2 configuration, (d) 1ML Na-adsorbed surface, (e) 0.5ML K-adsorbed surface with the diagonal configuration (Eads = -1.92 eV/atom), though the row-ordered 2x1 structure is also favorable (E_{ads} = -1.13 eV/atom), and (f) 0.5ML Cs-adsorbed surface, where the row-ordered surface is thermodynamically unstable ($E_{ads} > 0$). In this and subsequent figures, carbons are blue, oxygens are red, metal atoms are yellow.

Table 1 shows the structures from Figures 1 and 2, grouped by coverage. For a full monolayer coverage, the adsorption energy of lithium atoms (-3.64 eV/atom) is more than twice that of sodium (-1.62 eV/atom). Although a full monolayer is in principle also possible for potassium and caesium, such structures are not thermodynamically favorable ($E_{ads} > 0$). Thus lithium and sodium form a unique pair (Figure 1(b) and (d)). Within that pair, the small size of lithium is reflected in the tight incorporation of the adsorbate atoms into the surface structure with angles between the Li-O vector and the surface normal of 68.6° and 83.1° respectively for each of the two Li atoms in the unit cell. In contrast, sodium atoms protrude significantly with angles of 51.7° and 57.5° between the Na-O vectors and the surface normal, consistent with the larger atomic radius of Na. In both cases, although the overlayer structure is 1x1, it is important to note that the underlying first row carbons exhibit a 2x1 dimer reconstruction and the two Li/Na atoms in each 2x1 unit cell are inequivalent. Where this is so, Table 1 shows the data for each unit cell adsorbate separately.

There is much more variety in the half-monolayer structures. For example, there are three Mg adsorbate structures at this coverage for which $E_{ads} < 0$. The 0.5ML Mg-adsorbed surfaces show many features in common with the 1ML Li-adsorbed surface, with tight structural incorporation of Mg adsorbates and large adsorption energies, consistent with the structural similarity between the solid-state chemistries of Li and Mg. The most stable structure occurs for a √2x√2 Mg overlayer where one Mg atom per 2x2 unit cell lies between the dimer rows and the other sits on the dimer row forming a zig-zag arrangement along the dimers. The other two structures (row-ordered) have the Mg atoms either both on the dimer row or both between them – the latter is shown in Figure 2a. The three 0.5ML Mg cases vary significantly in both adsorption energy and electron affinity. In the rest of the work we concentrate on the most stable structure (√2x√2) since one would expect experimentally this would be the most significant.

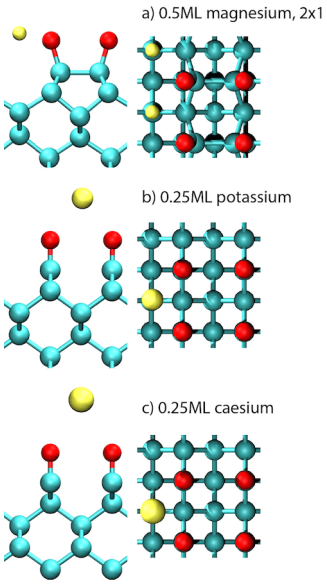

Figure 2. Further structures of interest. (a) The 0.5ML row-ordered Mg-adsorbed surface with adsorbates between the dimer rows, (b) the 0.25ML K-adsorbed surface and (c) the 0.25ML Cs-adsorbed surface. The latter two are more stable than their higher-coverage counterparts due to reduced adsorbate-adsorbate interaction.

Table 1. Properties for the family of surfaces studied in the present work*

Coverage (ML)	Adsorbate	Surface Unit Cell	E_{ads} (eV)	I (eV)	χ (eV)	d_{CO} (Å)	d_{XO} (Å)	θ_{XO} (°)
-	(clean O)	1x1	-	7.80	2.33	1.51	-	-
1	Li	2x1	-3.64	1.97	-3.50	1.40	1.89/1.83	68.6/83.1
1	Na	2x1	-1.62	4.05	-1.42	1.34	2.26/2.14	51.7/57.5
0.5	Mg	2x1 between dimer rows	-3.43	2.19	-3.28	1.39	1.86	80.7
0.5	Mg	2x1 on dimer row	-2.80	3.29	-2.18	1.39	1.96	67.3
0.5	Mg	2x2 (√2x√2)	-3.92	2.70	-2.77	1.39	1.93/1.87	65.2/76.4
0.5	Na	2x1	-2.07	4.19	-1.28	1.25	2.24	53.3
0.5	Na	2x2 (√2x√2)	-2.41	4.17	-1.30	1.25	2.26	52.4
0.5	K	2x1	-1.14	4.06	-1.41	1.25	2.47	46.5
0.5	K	2x2 (√2x√2)	-1.92	4.16	-1.31	1.24	2.53	45.0
0.5	Cs	2x2 (√2x√2)	-1.23	3.60	-1.87	1.25	2.76	40.5
0.25	K	2x2	-2.44	3.03	-2.44	1.23	2.49	46.6
0.25	Cs	2x2	-2.19	3.06	-2.41	1.23	2.82	39.4

*Symbols are as follows: adsorption energy per adsorbate E_{ads}, ionization energy I, electron affinity χ, carbon-oxygen bond length d_{CO}, adsorbate-oxygen bond length d_{XO} and the adsorbate-oxygen-surface normal angle θ_{XO}. The latter is a measure of the structural incorporation of the adsorbate into the surface.

We note that the adsorption energies shown in Table 1 are the average per adsorbate with respect to the bare oxygenated surface and consequently can be somewhat misleading when adsorbate interactions are strong as for the heavier alkali metals. For example, consider the values for 0.25ML of Cs (Figure 2c) versus 0.5ML in the √2x√2 structure (Figure 1f), -1.23 eV versus -2.19 eV. This difference reflects an averaging: with respect to the 0.25ML surface, the adsorption energy of the second Cs atom per 2x2 unit cell is just -0.27 eV, almost an order of magnitude less than the first. Adsorbate interactions for 0.5ML Cs adsorption on oxygen-terminated diamond were examined in great detail by Pickett.[17] Hence, in this work, we focus on lower coverages for the heavier alkali metals, which we will show share some features in common with the lighter alkali metals in terms of electronic structure.

Interactions between adsorbates are also significant for sodium. The row and diagonal 0.5ML Na structures have larger adsorption energies than the 1ML case, with the diagonal structure lower in energy than the row structure. This is reasonable given that the nearest adsorbate neighbors in the row structure are closer than in the diagonal. We have used the 1ML structure as the primary Na surface under consideration in this work; it represents a transition between the Li/Mg and the K/Cs families and has a unique set of metallic surface states that may well be of interest experimentally.

The C-O bond length varies systematically with the increasing size of the alkali metal adsorbate. The clean oxygen-terminated surface has a C-O bond length slightly longer than expected for ether linkages at 1.50 Å. At the other extreme, both Cs-adsorbed and K-adsorbed surfaces have C-O bond lengths much closer to a conventional carbonyl bond at 1.23-1.25 Å. This is consistent with the lack of dimer reconstruction in these cases. The intermediate cases (Li, Mg and Na) all have C-C dimers and correspondingly the C-O bond length lies in the range 1.34-1.40 Å. Especially in the cases of Li and Mg this indicates the C-O character is much closer to a single bond.

For further examination we consider a reduced set of representative adsorbate systems. Experimental considerations suggest we prioritize structures with maximal coverage, lowest binding energy and most negative electron affinity. On that basis, the surfaces of most interest are as follows: the reference 1ML lithiated surface, the √2x√2 magnesium 0.5ML surface, the 1ML sodium surface and the 0.25ML potassium and caesium adsorbed surfaces.

2. Averaged electrostatic potentials and surface dipoles

Figure 3 shows the variation of the average electrostatic potential in plane perpendicular to the slab surface for the 1ML Li and 0.5ML √2x√2 Mg surfaces. A structural overlay is present to show the relative positions of the atoms within the slab structure including the adsorbates. The electrostatic potential is the Hartree (electronic) potential plus the attractive potential generated by the pseudopotentials representing the ionic sites. The exchange-correlation potential is excluded because it is poorly represented in the vacuum gap where the charge density is very low and consequently makes it difficult to locate an unambiguous

vacuum level. The exclusion of the exchange correlation potential does not affect the calculated ionization energy or electron affinity because these calculations are based on energy differences rather than total energies.

The key features of interest in Figure 3 are threefold. First, there is a clear vacuum level set to zero eV in each simulation. Second, within the bulk there is a weakly modulated potential imposed on a well of depth ~13-15 eV. Third, joining these two regions is a strongly oscillating potential that corresponds to the surface dipole induced by the adsorbates. These oscillations contrast strongly with the equivalent for hydrogen-terminated diamond.[37] In both Figures 3 and 4 it is important to note that the potential is that felt by the electrons and since, by Poisson's equation:

$$\nabla^2 V = -\frac{\rho}{\varepsilon} \quad (3)$$

the curvature of the potential gives the charge density. Hence the points of maximum curvature – the peaks and troughs in the surface dipole, for example - correspond to local extrema in charge density. With the current sign convention, the peaks correspond to higher local negative charge accumulation and the troughs to regions of relatively high positive charge. Thus in Figure 3, for example, the component of the dipole perpendicular to the surface is oriented with the positive side facing the vacuum. The final point of note is that while the positive side of the dipole is centered on the Li/Mg adsorbates, the negative side of the dipole is centered partway along the C-O bonds and not on the atomic nuclei. This is important for the classification of the dipole and will be discussed later in connection with the bond orientations of these metal adsorbates relative to those of the larger Na, K and Cs.

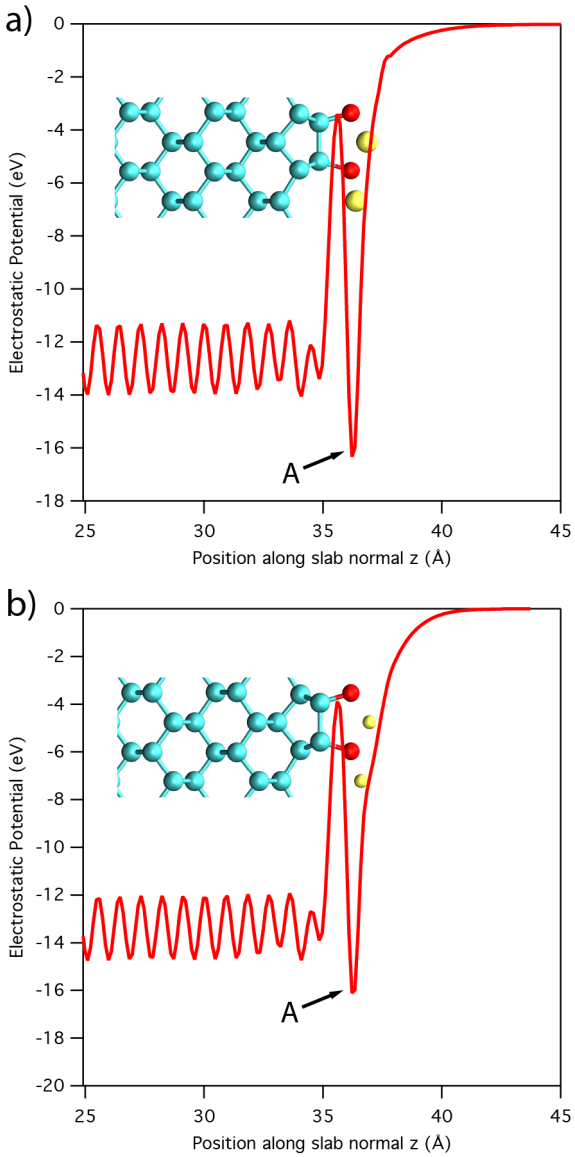

Figure 3. Plane-averaged electrostatic potential with a structural overlay to show the position of the surface atoms relative to the surface dipole features. (a) The 1ML Li-adsorbed surface, (b) the 0.5ML √2x√2 Mg-adsorbed surface.

Figure 4 shows the equivalent plane-averaged potentials for the 1ML Na and 0.25ML Cs surfaces. Unlike the plots in Figure 3, there are two sets of oscillations and hence two dipoles at the surface. The oscillations are roughly of equal size for Na (Figure 4a) but not for Cs (Figure 4b). For Cs the potential is positive on the positive side of the second dipole due to the absence of the exchange-correlation potential. Note the shift in the minimum potential at the oxygen site (labeled as feature A in Figures 3 and 4) between the Li/Mg surfaces and those of Na and Cs.

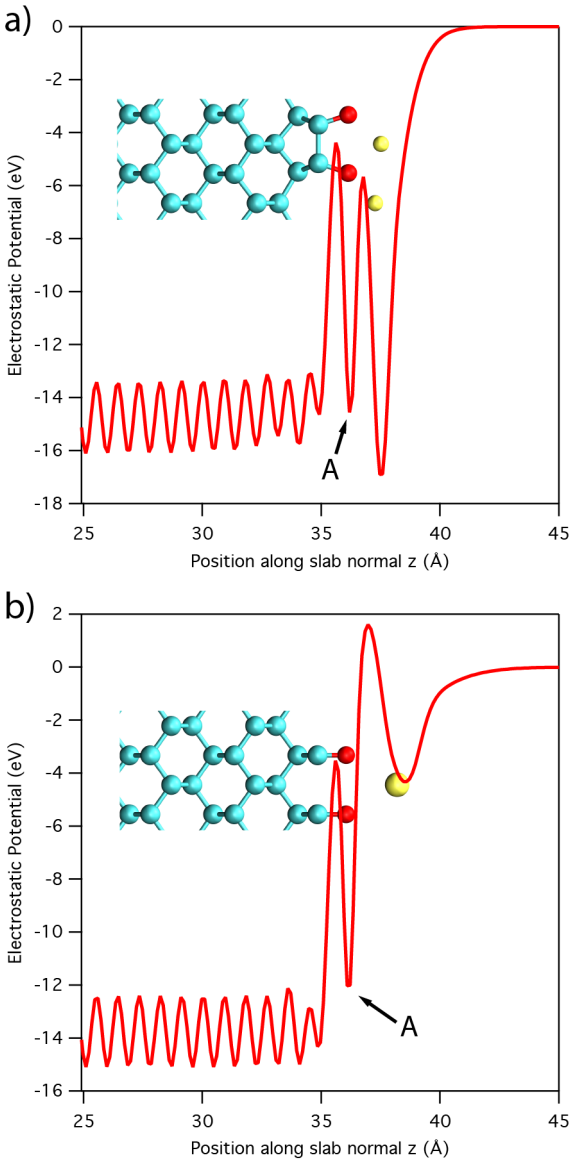

Figure 4. Plane-averaged electrostatic potential for (a) the Na-adsorbed 1ML surface and (b) the Cs-adsorbed 0.25ML surface. The K-adsorbed 0.25ML surface is essentially identical to that of Cs. These heavier alkali metals show very significantly different dipole structures to the Li and Mg cases of Figure 3.

3. Density of States and Surface Band Structure

Figure 5 compares the surface electronic structure of the bare oxygenated structure with those of the 1ML Li and Na adsorbed surfaces. The band structures are overlaid on the projected bulk band structure. Energy alignment to the projected bulk bands is achieved by first aligning the bulk bands such that the VBM is zero, then shifting the overlaid bands from the slab calculation such that the bottom of valence band is aligned in each case. We use the bottom of the valence band because it is unambiguous in all simulations. A point to note is that this method gives excellent alignment with the CBM, as can be seen in all the band structure plots near 4.1 eV. However, the nominal VBM apparent in the slab calculations is approximately 0.5 eV lower, i.e., the slab calculation has a narrower valence bandwidth. This is likely to be a consequence of the finite slab thickness. The ionization energies computed earlier do not rely on the slab bandwidth and hence avoid this issue.[35] In the band structures, we can still distinguish occupied and unoccupied states by counting electrons (finite band gap) or by the self-consistent Fermi level for metallic states.

The oxygenated surface (Figure 5a) has a band structure similar to that reported previously[33] consisting of occupied and unoccupied bands arising from the oxygen lone pairs intruding upon the band gap. The dispersion of the main branches and the band crossings are slightly different along the Γ-X and Γ-Y directions, reflecting the symmetry of the ether bridges. The reciprocal space directions Γ-X and Γ-Y relative to the real-space lattice are indicated in Figure 1. The oxygen atoms form ether bridges parallel to the Γ-Y direction. The occupied surface states are the solid-state equivalent of the oxygen non-bonding lone pairs – we subsequently call them lone pair states for simplicity. Figures 5b and 5c show features common to all the alkali-adsorbed surfaces. These are seen most simply in the case of lithium, where the lone pair states at the surface are lowered in energy and the first unoccupied surface state is s-like, consistent with the donation of the Li 2s electron to the surface. The lone pair states also have altered dispersion: the states remain p-like along Γ-X but are essentially flat (localized) along Γ-Y. This altered dispersion is observed for all the adsorbed surfaces considered here regardless of whether or not there is also a shift in in the energy of the states and reflects the change in the oxygen-surface bonding from ether bridges to C-O-X or C=O functionality.

For Na the situation is slightly more complicated: the system is metallic and the computed Fermi level is shown in Figure 5c as a dashed horizontal line. The lone pair states have the same dispersion as in the lithiated case but they are not shifted to lower energies, whereas the *s*-like state, unoccupied in the lithiated case, is now below the Fermi level. It is not clear if this is an artifact of DFT which is known to incorrectly predict metallic behaviour for some small band gap systems due to the neglect of on-site Coulomb repulsion. If not, the metallic states may arise from hybridization between the Na 3*s* states and the O 2*p* states coupled with direct Na-Na interaction due to close packing.

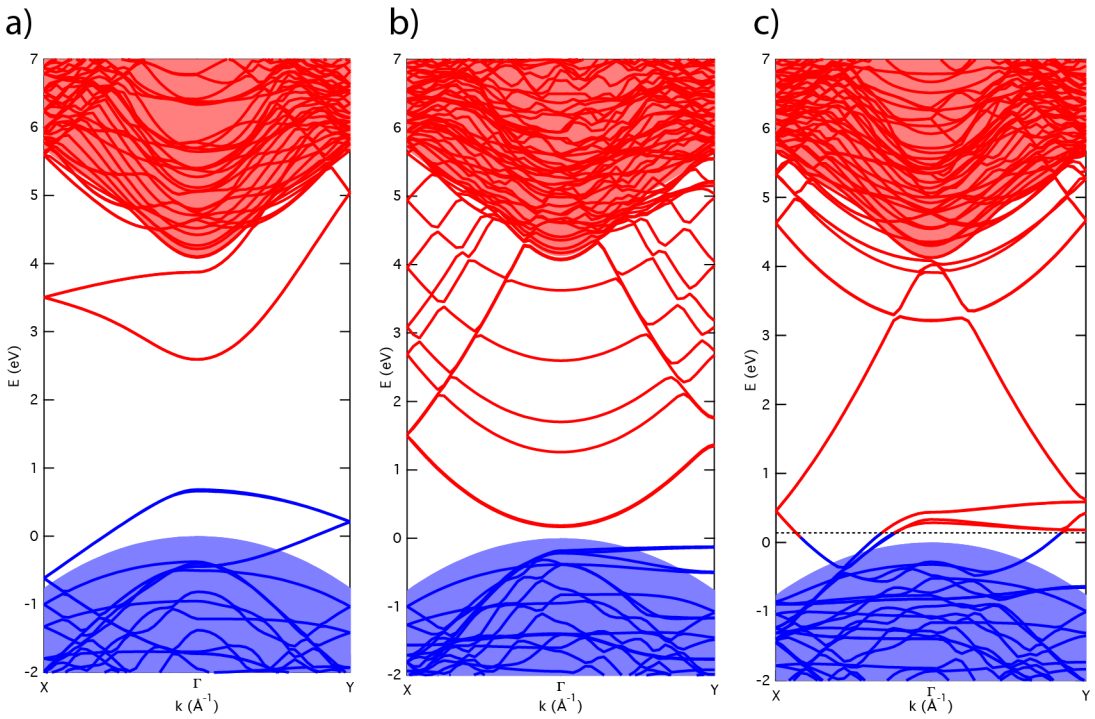

Figure 5. Surface band structures computed along the X-Γ-Y path for a 2x2 unit cell for (a) the clean ether-bridge oxygen-terminated surface, (b) the 1ML Li-adsorbed surface and (c) the 1ML Na-adsorbed surface. In (c) the system is metallic at the surface and the Fermi level is indicated (dashed horizontal line). In this and subsequent figures, occupied and unoccupied states are coloured blue and red respectively. Shaded areas reflect the projected bulk bands.

Figure 6 shows the band structures for the 0.5ML √2x√2 Mg surface and the 0.25ML K and Cs surfaces. The electronic structure for the Mg surface is analogous to that of the Li-adsorbed surface at twice the coverage. Note that the branch of the Mg 3*s* state in the first Brillouin zone now cuts through the Fermi level – the system is metallic at the level of calculation. Given the known limitations of DFT band gaps this result must be taken with care. In the set of 0.5ML Mg surfaces the status as a metal for the diagonal structure is unique – both 2x1 structures are semiconducting with a band structure essentially the same as that of 1ML Li.

In contrast to the Mg case, the K and Cs band structures show clear similarities with the 1ML Na surface in Figure 5c. As with the Na-adsorbed surface the lone pair states of the oxygen are not lowered in energy but in the 0.25ML K and Cs surfaces the *s* state does not overlap with the occupied states and the surfaces are both narrow band gap semiconductors.

The use of atom-projected density of states (PDOS) allows a more quantitative assignment of spectral features to particular atomic species. Figure 7 shows PDOS computed for the oxygenated diamond surface, the 1ML Li-adsorbed and Na-adsorbed surfaces. The individual PDOS spectra arise from projections onto the following atomic sites: bulk carbon (taken from the middle of the simulation slab), surface carbon (immediately bonded to oxygen), oxygen and the adsorbate species. The PDOS spectra are aligned such that the bulk VBM is at zero, as with the band structures. Vertical lines indicate the highest occupied state or the Fermi level depending on whether the system is semiconducting or metallic.

While as expected the bulk carbon PDOS is essentially identical in all spectra, the surface carbon and oxygen PDOS vary significantly between the adsorbed surfaces and the bare oxygenated surface. This reflects the change in structure from *sp*-bonded ether bridges to the more ionic Li-O-C and Na-O-C complexes. Again it can be seen that the occupied oxygen PDOS above the valence band maximum is lowered in energy (shifts to the left in Figure 7) for Li, whereas the Fermi level cuts through these states (partial occupation) for Na. In both Figure 7b and 7c it can be seen that the dominant unoccupied states intruding on the bulk band gap arise from the alkali adsorbates, again in contrast to the clean oxygenated surface where the surface carbon and oxygen are responsible. As with the band structures the density of states for Li and Na are broadly similar, but for Na the unoccupied states extend lower in energy and the oxygen occupied states extend higher, consistent with the increased charge transfer expected for Na compared to Li based on their relative electronegativities.

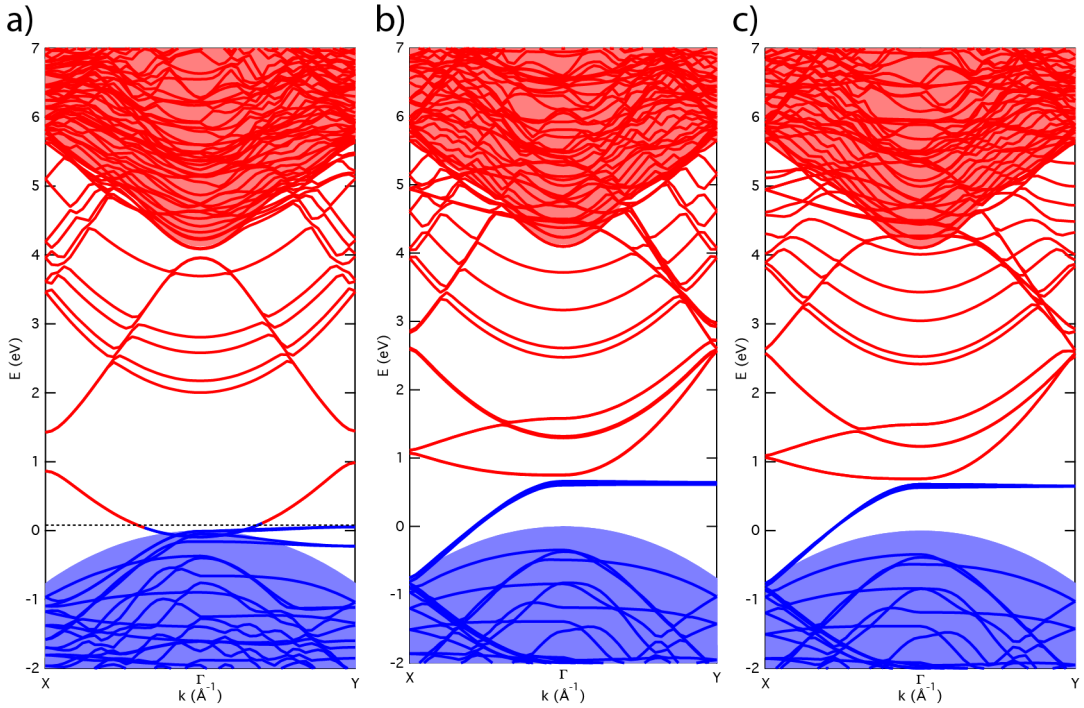

Figure 6. Band structures for (a) 0.5ML √2x√2 Mg-adsorbed surface, (b) the K-adsorbed 0.25ML surface and (c) Cs-adsorbed 0.25ML.

Figure 8 shows the projected density of states for the 0.5ML √2x√2 Mg-adsorbed surface (Fig. 8a) and the 0.25ML K and Cs-adsorbed surfaces (Figs 8b and 8c respectively). The Mg-adsorbed surface has essentially the same PDOS as that of the Li-adsorbed surface except that the unoccupied states show more structure in the band gap. In marked contrast, the two heavy alkali metals show a wholly distinct PDOS. For both K and Cs, the bulk band gap is dominated by several sets of surface bands from oxygen alone, C-O antibonding levels and from the alkali itself. There is also evidence of higher core levels (e.g. 5*s* and 5*p* for Cs) interacting with the 2*s*-like states of the surface carbon and oxygen. This is analogous to that found by Pickett for a similar Cs-adsorbed oxygenated diamond surface.[17]

Discussion

It is immediately evident from the structures for lithiated and magnesiated C(100)-(1x1):O that any net dipole moment perpendicular to the surface arising from charges situated on atomic sites must be small because the adsorbates are well-incorporated into the surface structure. In contrast, surfaces with various coverages of adsorbed sodium, potassium and caesium have a different dipole structure, with the positive alkali ion some distance from the surface. Nevertheless, the ionization energy of the lithiated and magnesiated surfaces is significantly less than all the others leading to a larger NEA and suggesting the presence of a stronger surface dipole.

To unravel this apparently counter-intuitive result we first consider the average planar electrostatic potential V_{elec} taken along the surface normal direction for the different structures. In a plot of V_{elec} versus the slab z-coordinate, the dipole potential is apparent at the interface between the deep bulk potential and the vacuum level. In the case of lithium or magnesium-adsorbed surfaces (Figures 3a and 3b), the negative side of the dipole (corresponding to electron accumulation) is centered over the C-O bonds and the positive side over the Li-O or Mg-O complexes which are almost parallel to the plane of the surface as seen earlier. The caesium-adsorbed and potassium-adsorbed surfaces exhibit a similar dipole between the C-O bonds and the Cs-O/K-O complexes (Figure 4b for Cs, representative) but *additionally* show a dipole between the Cs/K sites and the Cs-O/K-O bonds. The consequence is that the positive side of the first dipole, marked as feature A in Figures 3 and 4, is partially cancelled out by the negative side of the second, and the net dipole is reduced. The sodium-adsorbed surface shows two dipoles as with caesium but the cancellation between the two is less significant (Figure 4a). On this basis we associate the lithium and magnesium cases as one group of surface dipole, potassium and caesium as another, with sodium intermediate.

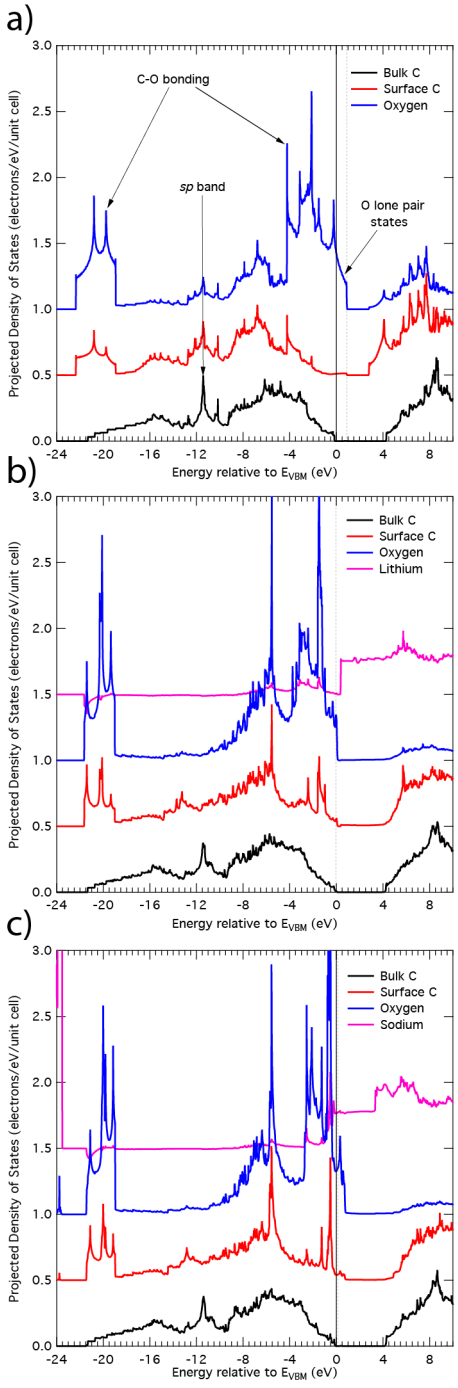

Figure 7. Atom-projected partial density of states for (a) clean ether-bridged oxygen-terminated diamond, (b) the 1ML Li-adsorbed surface and (c) the 1ML Na-adsorbed surface. A vertical dashed line indicates the Fermi level in (c) and the highest occupied state for (a) and (b).

In our earlier paper[22] we argued that the charge separation seen for the Li surface and here also for Mg results from the oxygen lone pair states overlapping in energy with the valence band, i.e. covalence. The energy lowering leading to this overlap arises from the presence of the positive charge of the Li sites. The structural differences between the lithium-adsorbed surfaces, where the Li is in almost the same surface plane as the O sites, and those with heavier alkali adsorbates suggest that this dipole mechanism would be much less effective for the heavier species since they are much further from the plane of the surface oxygens. This can be directly observed in the band structure, where the occupied surface states associated with oxygen are lowered in energy for both Li and Mg but critically not for K and Cs, again with Na intermediate. The change in energy is independent of the change in *dispersion* – in all adsorbed band structures, the dispersion of the lone pair states is essentially identical, only the energy position relative to the VBM changes. We argue here that the change in dispersion (relative to the bare oxygenated surface) relates to *structure* (the breaking of the ether bridges), whereas the change in energy position relates to the local potential environment induced by the adsorbates. Since the heavier alkalis cannot incorporate into the surface as effectively, they have a small effect on the energy level of the lone pair states. The result is that a significant fraction of negative charge is located between the oxygen and alkali metal sites. Conversely in the case of Li and Mg the surface incorporation leads to the lone pair states being lowered in energy. The subsequent overlap with the valence band leads to negative charge enhancement around the C-O bonds rather that at the O sites, giving the spatial charge separation perpendicular to the surface normal necessary for a strong dipole.

The unoccupied states intruding into the band gap are also of interest. For Li, Mg and Na the atom-projected DOS show that these states primarily result from the *s*-like states of the adsorbates themselves. In the case of Na the unoccupied 3*s* states intrude into the diamond valence band and mix strongly near Γ, leading to a metallic surface. We reiterate here that the DFT result of a metallic surface is not conclusive given the known limitations of DFT with respect to the band gap. However, we can make the following argument: the DFT-predicted bulk band gap in the present study is 4.1 eV, compared to the experimental value of 5.5 eV.[36] Thus, a scissor correction (rigid shift of unoccupied states) of approximately 1.4 eV is required to correct the computed values to agree with experiment. The scissor correction to GGA eigenvalues is known to give good agreement with both experiment and higher levels of theory in the case of diamond.[38] For the semiconducting Li-adsorbed surface, for example, this results in a surface band gap of approximately 1.6 eV. A crude manipulation of the energies of Na-adsorbed surface states, scissor-correcting the 3*s* states based on the Na-projected PDOS leads to a minimum 3*s* band position of between -1.3 to 0.6 eV. Thus it remains ambiguous as to whether the surface would really be metallic, and experimental examination is required. The Mg-adsorbed case is somewhat clearer: the 2*s* states only just overlap with the valence band and it may well only be a metal at the DFT level.

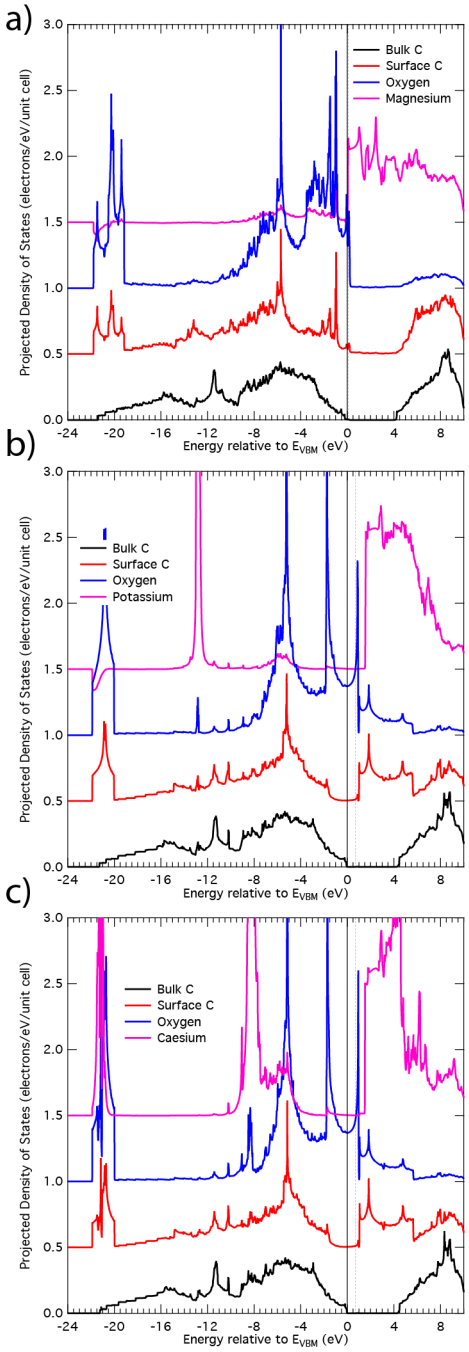

Figure 8. Atom-projected partial density of states for (a) 0.5ML √2x√2 Mg-adsorbed surface, (b) the 0.25ML K-adsorbed surface and (c) the 0.25ML Cs-adsorbed surface. Note here that oxygen PDOS extends higher in energy than the bulk VBM. A vertical dashed line indicates the Fermi level in (a) and the highest occupied states in (b) and (c).

The similar dispersion of the oxygen lone pair states for all adsorbate structures arises from the breaking of the ether bridges. The nature of the terminations varies with the adsorbate. For Li and Mg the primary contributor is the C-O-X functionality with a C-O single bond and C-C dimer bond, whereas for Cs and K the primary contributing state consists of carbonyl-bonded oxygen, no C-C dimer bond and a X-O charge transfer establishing the conventional dipole. We illustrate these possibilities in Figure 9. We emphasize the interplay between geometric and electronic structure that leads to the separation of these systems into two groups. It is worth comparing the effects of alkali metal adsorption to that of OH-terminated diamond (100) as considered by Sque, et al[33] at the DFT level. In the case of OH, the dispersion of the occupied states (particularly the lone-pair electrons) agrees reasonably well with those of the present study for both the ether-bridge and OH-terminated surfaces. This is consistent with the view that the change in the dispersion is due to the breaking of ether bridges. The relaxed OH structure, however, is somewhat different to the alkali adsorption structures in that the hydrogen atoms engage in hydrogen-bonding with the lone pairs of adjacent oxygen atoms. This results in the formation of hydrogen-bonded rows along the dimers rather than, for example, the interlocking square lattices of O and Li atoms in the 1ML "LiO"-terminated surface. One would expect this would result in a significantly different surface charge density distribution, surface dipole and consequently electron affinity. It turns out that the OH-terminated surface is predicted to have a small NEA of -0.55 eV, almost an order of magnitude smaller than the lithium or magnesium adsorbed surfaces.

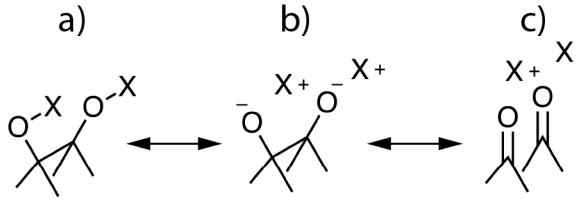

Figure 9. Bonding scheme for the X-O-C complexes observed in this work. In general, all structures share elements of the alcohol-like covalent bonding (a) and the carbonyl ionic bonding (c). However, adsorbate size impacts the relative contribution of these structures, leading to Li and Mg being more like (a), K and Cs more like (c) and Na the intermediate case (b).

The projected density of states spectra allow examination of the adsorbate-oxygen interaction further into the valence band. For clean oxygenated diamond, the bulk *sp*-band seen in ultraviolet photoelectron spectroscopy appears prominently in a DFT calculation at around -11.4 eV for bulk carbon, surface carbon and surface oxygen. This suggests some degree of continuity in the nature of the C-O bonding on C(100). C-O 2*p*-like bonding appears in the region -2 to -4 eV. The oxygen lone pair states lie between -2 eV and 0.9 eV. It is important to note that these states extend quite significantly above the bulk VBM and hence in a boron-doped diamond would cause band-bending. We believe this to be why boron-doped, oxygen-terminated diamond is usually found to have E_F-E_{VBM} = 0.7-1.0 eV at the surface.[13,15,39]

Even disregarding the adsorbate-projected PDOS, the surface carbon and oxygen PDOS for the adsorbed surfaces are wholly different to the clean case. For example,

consider the Li-adsorbed surface (Fig 7b). The *sp* band does not appear in either surface species and there are no surface states extending past the bulk VBM. Instead, a prominent bonding state appears at just below -5 eV, with further C-O bonding states between -1.0 and -2.4 eV. The features are also seen in the Mg-adsorbed surface (Fig 8a) albeit with a nominally metallic surface structure. The adsorbate-projected PDOS for both Li and Mg show the band gap unoccupied states are wholly related to the adsorbate with no involvement from surface oxygen or carbon.

Although structurally the 1ML Na-adsorbed surface is similar to that of Li-adsorbed diamond through dimer formation and some adsorbate incorporation into the surface, electronically there are clear similarities to the heavier alkali metals. The densities of states for both K and Cs (Figs 8b and 8c) show significantly different structures in the 2.5 to -2.5 eV region and a very high oxygen density of states above the bulk VBM. There are indications of both features to a lesser degree in the Na-adsorbed surface, supporting our assignment of Na-adsorbed oxygen-terminated diamond as the transition point between two groups of adsorbate system.

Common to all the adsorbed structures and distinct from the clean ether-bridge oxygen-terminated surface is the strong PDOS feature around -5.3 eV present on both the surface carbon and surface oxygen sites. The fact that this is not seen on the clean surface nor in the bulk and concurrent with the disappearance of the *sp*-band feature at the surface leads us to assign this as *characteristic* of the carbon-oxygen bonding structure seen in the C-O-X complexes of the relaxed adsorbed surfaces. Since in all the adsorbed surfaces, the relaxed state involves the breaking of C-O-C ether bridges, there are practical consequences for the possible generation of many of these surfaces. For example, it is seen experimentally that in the case of lithium it is necessary to anneal after deposition in order to induce NEA; the concurrent electronic and chemical shifts were interpreted as resulting from a change from a metastable adsorption site to the thermodynamically preferred site under annealing.[13]

The adsorption energy of Li on the oxygenated surface is high enough that high annealing temperatures can be sustained to overcome the kinetic barrier between such sites without desorbing the Li atoms, as we have shown experimentally.[13] However, although this may also be so for Mg, the adsorption energies for the heavier alkali metals are typically less than 2-2.5 eV and it is not clear that high annealing temperatures can be withstood for a similar activation process. Indeed, the reported stability of Cs on the oxygenated diamond surface suggests an upper limit of approximately 500°C.[18]

On the other hand, since it is clear that the heavier alkalis chemically interact with the surface in significantly different ways it is possible that for these surfaces the need for annealing (or at least high temperature annealing) is reduced. More experimental work on this topic is justified; whilst the Li-adsorbed surface is outstanding for certain applications, it may be that the heavier alkalis have advantages for applications where annealing is not feasible, or where the metallic electronic structure is desirable. Other examples of interest are the Mg-adsorbed surface that gives essentially the same electronic structure and predicted negative electron affinity as the lithiated surface. Magnesium is somewhat easier to deposit and investigate using conventional photoemission techniques than lithium and may be a more practical adsorbate for applications. Finally, it is of interest to determine experimentally whether the Na-adsorbed oxygen-terminated C(100) surface is in fact metallic, as well as carrying out the calculations beyond the DFT level. The quality of the oxygen termination will no doubt be critical: it is an ongoing challenge to develop an experimental method for cleanly oxygen-terminating diamond without roughening the surface. However, the potential for a new low-dimensional system on diamond to complement the p-type hole layer formed via surface transfer doping would be of both fundamental and practical interest.

Conclusions

We have shown that Li- and Mg-adsorbed oxygen-terminated diamond has unique electronic properties resulting from the interplay between geometric and electronic structure in determining the surface dipole. These contrast strongly with the properties of K- and Cs- adsorbed surfaces that exhibit more conventional structural and electronic behavior. The key elements are as follows. First, tight structural incorporation of the adsorbate into the oxygen layer concomitant with a downshift in the electronic levels associated with oxygen lone pair electrons leading to covalence. Second, dipole formation whereby the negative side is primarily centered on the C-O bonds and the positive side is the adsorbate/oxygen overlayer. Finally, one requires no significant competing dipole arising from a traditional atom-centered dipole moment. The latter point is strongly tied to the physical structure of the adsorbate system because it is the tight incorporation of the adsorbates that reduces the adsorbate-oxygen dipole moment normal to the surface.

The heavier alkalis (including sodium) all fail to satisfy the above points and have smaller adsorption energies and higher ionization energies when adsorbed onto the C(100)-(1x1):O surface. In spite of this, the Na-adsorbed surface is predicted at the DFT level to be metallic at full monolayer coverage and may be of use for surface electronics. All the surfaces considered here are predicted to possess true negative electron affinity of varying degree, with the biggest effect seen for the lithium and magnesium-adsorbed surfaces. Combined with their relatively high adsorption energies, these surfaces are likely to be the most useful for applications requiring a robust NEA surface.

AUTHOR INFORMATION

Corresponding Author

*Kane O'Donnell, kane.odonnell@curtin.edu.au.

ACKNOWLEDGMENT

This work was supported by the Multi-modal Australian Sciences Imaging and Visualisation Environment (MASSIVE) (www.massive.org.au). This work was carried out using the computational facilities of the Advanced Computing Research Centre, University of Bristol - http://www.bris.ac.uk/acrc/. KOD thanks Lothar Ley (Erlangen) for helpful discussions regarding electron affinity.

REFERENCES

(1) Himpsel, F.; Knapp, J.; VanVechten, J.; Eastman, D. *Phys. Rev. B Condens. Matter* **1979**, *20*, 624.

(2) Chang, X.; Wu, Q.; Ben-Zvi, I.; Burrill, A.; Kewisch, J.; Rao, T.; Smedley, J.; Wang, E.; Muller, E.; Busby, R.; Dimitrov, D. *Phys. Rev. Lett.* **2010**, *105*, 164801.

(3) Yater, J. E.; Shih, A. *J. Appl. Phys.* **2000**, *87*, 8103.

(4) Shih, A.; Yater, J.; Pehrsson, P.; Butler, J.; Hor, C.; Abrams, R. *J. Appl. Phys.* **1997**, *82*, 1860.

(5) Takeuchi, D.; Koizumi, S.; Makino, T.; Kato, H.; Ogura, M.; Ohashi, H.; Okushi, H.; Yamasaki, S. *Phys. Status Solidi A* **2013**, *210*, 1961–1975.

(6) Kataoka, M.; Zhu, C.; Koeck, F. A. M.; Nemanich, R. J. *Diam. Relat. Mater.* **2010**, *19*, 110–113.

(7) Di Zhu; Zhang, L.; Ruther, R. E.; Hamers, R. J. *Nat Mater* **2013**, *12*, 836–841.

(8) Strobel, P.; Riedel, M.; Ristein, J.; Ley, L. *Nature* **2004**, *430*, 439–441.

(9) Russell, S. A. O.; Cao, L.; Qi, D.; Tallaire, A.; Crawford, K. G.; Wee, A. T. S.; Moran, D. A. J. *Applied Physics Letters* **2013**, *103*, 202112.

(10) Tordjman, M.; Saguy, C.; Bolker, A.; Kalish, R. *Adv. Mater. Int.* **2014**, 1300155.

(11) Edmonds, M. T.; Wanke, M.; Tadich, A.; Vulling, H. M.; Rietwyk, K. J.; Sharp, P. L.; Stark, C. B.; Smets, Y.; Schenk, A.; Wu, Q. H.; Ley, L.; Pakes, C. I. *J. Chem. Phys.* **2012**, *136*, 124701.

(12) Cui, J. B.; Ristein, J.; Ley, L. *Phys. Rev. Lett.* **1998**, *81*, 429–432.

(13) O'Donnell, K. M.; Edmonds, M. T.; Ristein, J.; Tadich, A.; Thomsen, L.; Wu, Q.-H.; Pakes, C. I.; Ley, L. *Adv. Funct. Mater.* **2013**, *23*, 5608–5614.

(14) Cui, J. B.; Graupner, R.; Ristein, J.; Ley, L. *Diam. Relat. Mater.* **1999**, *8*, 748–753.

(15) Maier, F.; Ristein, J.; Ley, L. *Phys. Rev. B Condens. Matter* **2001**, *64*, 165411.

(16) Maier, F.; Riedel, M.; Mantel, B.; Ristein, J.; Ley, L. *Phys. Rev. Lett.* **2000**, *85*, 3472–3475.

(17) Pickett, W. E. *Phys. Rev. Lett.* **1994**, *73*, 1664–1667.

(18) Loh, K.; Xie, X.; Yang, S.; Pan, J.; Wu, P. *Diam. Relat. Mater.* **2002**, *11*, 1379–1384.

(19) Baumann, P.; Nemanich, R. J. *Diam. Relat. Mater.* **1998**, *7*, 612–619.

(20) Baumann, P.; Nemanich, R. J. *J. Appl. Phys.* **1998**, *83*, 2072.

(21) Yater, J. E.; Shih, A. *Appl. Surf. Sci.* **1999**, *143*, 219–222.

(22) O'Donnell, K. M.; Martin, T.; Fox, N. A.; Cherns, D. *Phys. Rev. B Condens. Matter* **2010**, *82*, 115303.

(23) O'Donnell, K. M.; Martin, T. L.; Edmonds, M. T.; Tadich, A.; Thomsen, L.; Ristein, J.; Pakes, C. I.; Fox, N. A.; Ley, L. *Phys. Status Solidi A* **2014**, *211*, 2209-2222.

(24) Miyamoto, Y.; Miyazaki, T.; Takeuchi, D.; Yamasaki, S. *J. Appl. Phys.* **2014**, *116*, 124309.

(25) Clark, S.; Segall, M.; Pickard, C.; Hasnip, P.; Probert, M.; Refson, K.; Payne, M. *Z. Kristallogr* **2005**, *220*, 567–570.

(26) Hammer, B.; Hansen, L. B.; Nørskov, J. K. *Phys. Rev. B Condens. Matter* **1999**, *59*, 7413.

(27) Monkhorst, H.; Pack, J. *Phys. Rev. B Condens. Matter* **1976**, *13*, 5188–5192.

(28) Morris, A. J.; Nicholls, R. J.; Pickard, C. J.; Yates, J. R. *Computer Physics Communications* **2014**, *185*, 1477–1485.

(29) Pehrsson, P.; Mercer, T. *Surf. Sci* **2000**, *460*, 49–66.

(30) Loh, K.; Xie, X.; Lim, Y.; Teo, E.; Zheng, J.; Ando, T. *Surf. Sci* **2002**, *505*, 93–114.

(31) Rutter, M.; Robertson, J. *Phys. Rev. B Condens. Matter* **1998**, *57*, 9241–9245.

(32) Petrini, D.; Larsson, K. *J. Phys. Chem. C* **2007**, *111*, 795–801.

(33) Sque, S.; Jones, R.; Briddon, P. *Phys. Rev. B Condens. Matter* **2006**, *73*, 085313.

(34) Zheng, X.; Smith, P. *Surf. Sci* **1992**, *262*, 219–234.

(35) Fall, C.; Binggeli, N.; Baldereschi, A. *J. Phys. Condens. Matter* **1999**, *11*, 2689–2696.

(36) Dean, P. J.; Lightowlers, E. C.; Wight, D. R. *Phys. Rev* **1965**, *140*, A352.

(37) Van der Weide, J.; Zhang, Z.; Baumann, P.; Wensell, M.; Bernholc, J.; Nemanich, R. J. *Phys. Rev. B Condens. Matter* **1994**, *50*, 5803–5806.

(38) Edmonds, M. T.; Tadich, A.; Wanke, M.; O'Donnell, K. M.; Smets, Y.; Rietwyk, K. J.; Riley, J. D.; Pakes, C. I.; Ley, L. *Phys. Rev. B Condens. Matter* **2013**, *87*, 085123.

(39) O'Donnell, K. M.; Edmonds, M. T.; Ristein, J.; Rietwyk, K. J.; Tadich, A.; Thomsen, L.; Pakes, C. I.; Ley, L. *J. Phys. Condens. Matter* **2014**, *26*, 395008.

Insert Table of Contents artwork here